Electronic Supplementary Material (ESI) for Journal of Materials Chemistry A.

Nanoporous Mn-Based Electrocatalysts through Thermal Conversion of Cyano-Bridged Coordination Polymers toward Ultra-High Efficient Hydrogen Peroxide Production

Mohamed B. Zakaria[1,2,3], Cuiling Li[2]*, Malay Pramanik[2], Yoshihiro Tsujimoto[4], Ming Hu[5], Victor Malgras[2], Satoshi Tominaka[2], and Yusuke Yamauchi*[1,2,6]

1 *Faculty of Science and Engineering, Waseda University, 3-4-1 Okubo, Shinjuku, Tokyo, 169-8555, Japan.*

2 *World Premier International (WPI) Research Center for Materials Nanoarchitechtonics (MANA), National Institute for Materials Science (NIMS), 1-1 Namiki, Tsukuba, Ibaraki 305-0044, Japan.*

3 *Department of Chemistry, Faculty of Science, Tanta University, Tanta, Gharbeya 31527, Egypt.*

4 *Materials Processing Unit, National Institute for Materials Science, 1-2-1 Sengen, Tsukuba, Ibaraki 305-0047, Japan.*

5 *Department of Physics, East China Normal University, Physical Building, 500 Dongchuan Road, Shanghai, China*

6 *Australian Institute for Innovative Materials (AIIM), University of Wollongong, Squires Way, North Wollongong, NSW 2005, Australia*

E-mails: LI.Cuiling@nims.go.jp; Yamauchi.Yusuke@nims.go.jp

Homepage: http://www.yamauchi-labo.com

Figure S1

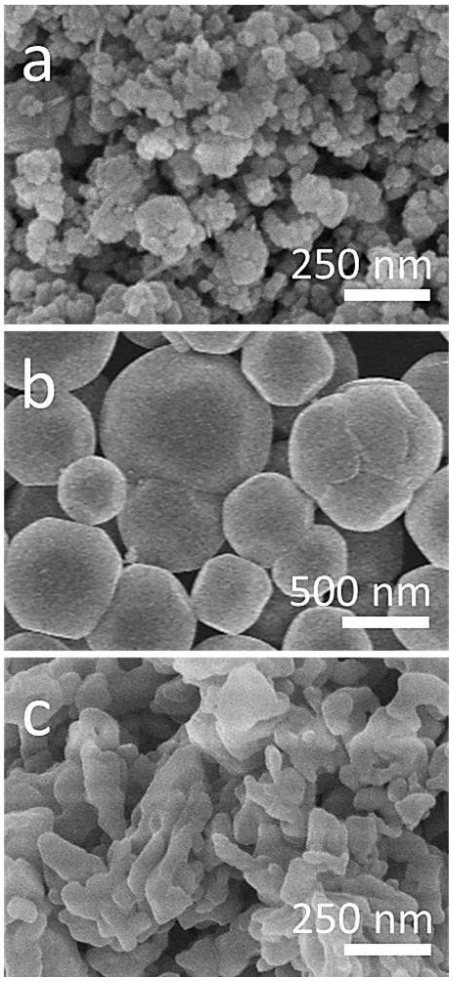

Figure S1 SEM images of the (a) MnCNMn, (b) MnCNCo, and (c) MnCNRu PBAs, prepared in the absence of TSCD.

Figure S2

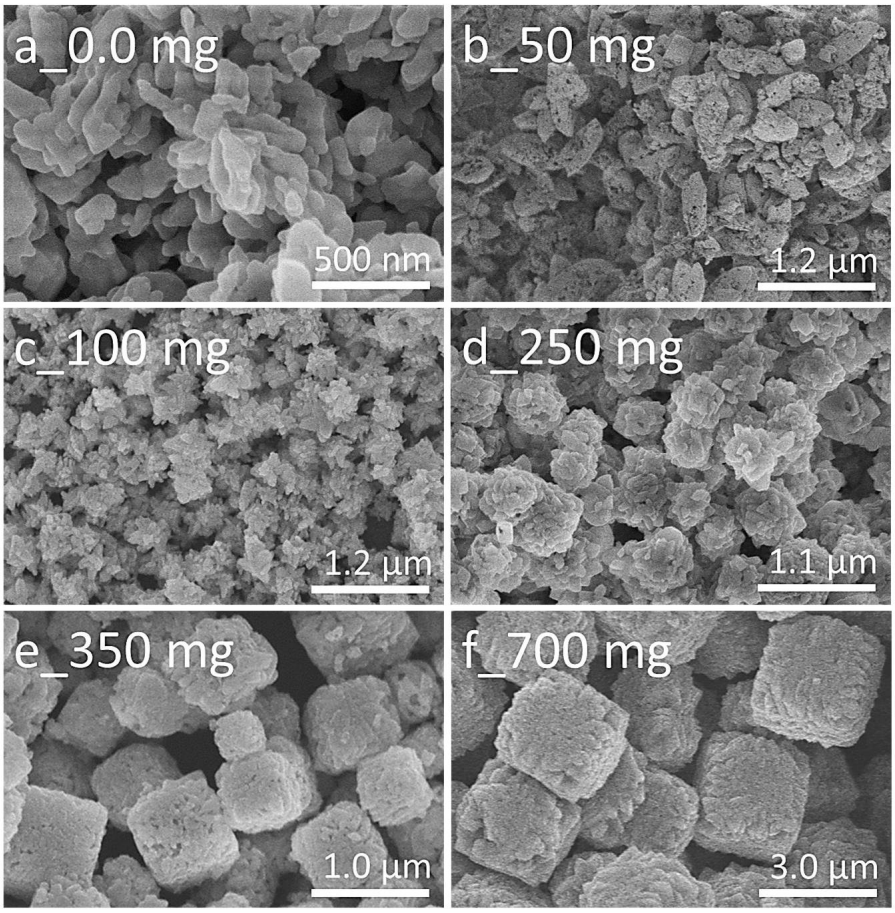

Figure S2 SEM images of the MnCNRu prepared with various amounts of TSCD.

Figure S3

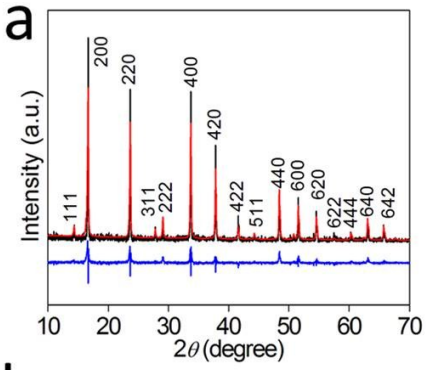

Crystal system	cubic
Space group	*Fm-3m*
a/Å	10.621 (4)
b/Å	10.621 (4)
c/Å	10.621 (4)
α/°	90
β/°	90
γ/°	90
V/ Å^3	1198.109
Z	1
λ/Å	1.5406
R_p	0.393
R_{wp}	0.468

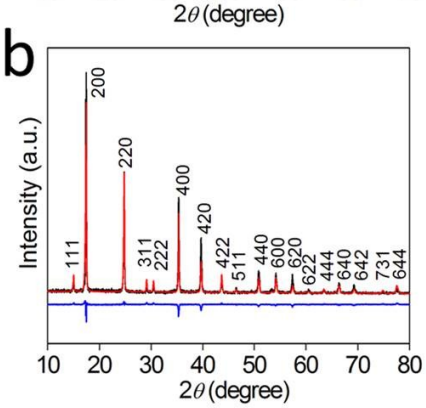

Crystal system	cubic
Space group	*Fm-3m*
a/Å	10.402 (5)
b/Å	10.402 (5)
c/Å	10.229 (5)
α/°	90
β/°	90
γ/°	90
V/ Å^3	1125.513
Z	1
λ/Å	1.5406
R_p	0.378
R_{wp}	0.446

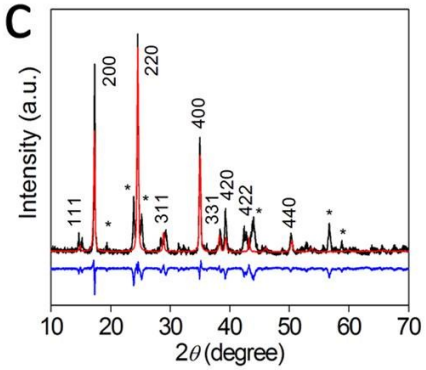

Crystal system	cubic
Space group	*Fm-3m*
a/Å	10.219 (3)
b/Å	10.219 (3)
c/Å	10.219 (3)
α/°	90
β/°	90
γ/°	90
V/ Å^3	1067.149
Z	1
λ/Å	1.5406
R_p	0.492
R_{wp}	0.579

Figure S3 Experimental XRD patterns (black line), computed XRD patterns (red line), and the residuals (blue line) of (a) MnCNMn, (b) MnCNCo, and (a) MnCNRu. The peaks indicated by (*) are generated from impurities.

Figure S4

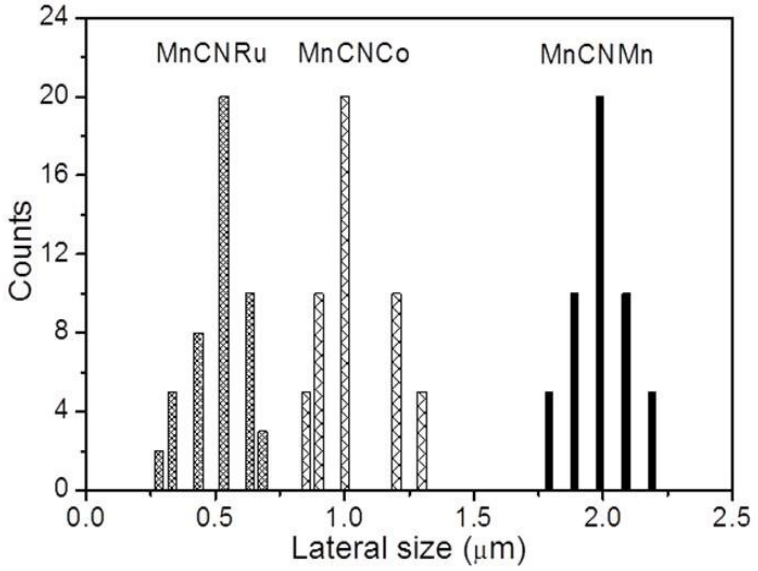

Figure S4 Particle size distributions obtained from TEM images of (a) MnCNMn, (b) MnCNCo, and (a) MnCNRu PBAs.

Figure S5

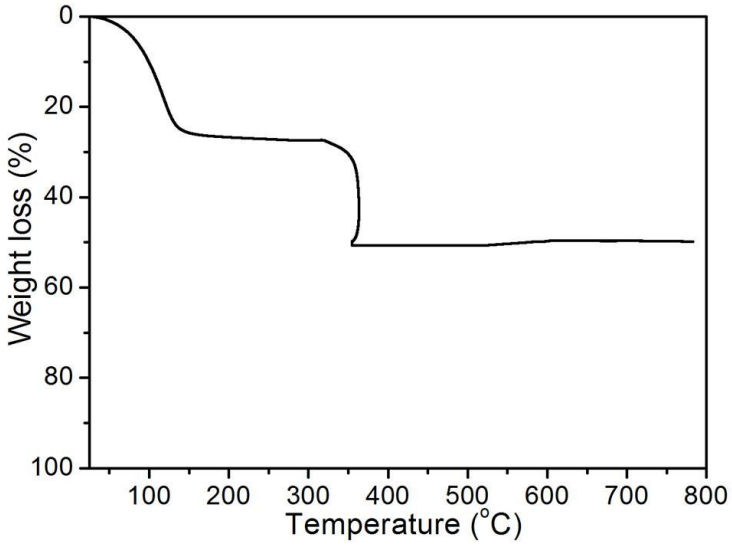

Figure S5 TG curve of MnCNCo at a heating rate of 5 °C min^{-1} from room temperature to 800 °C.

Figure S6

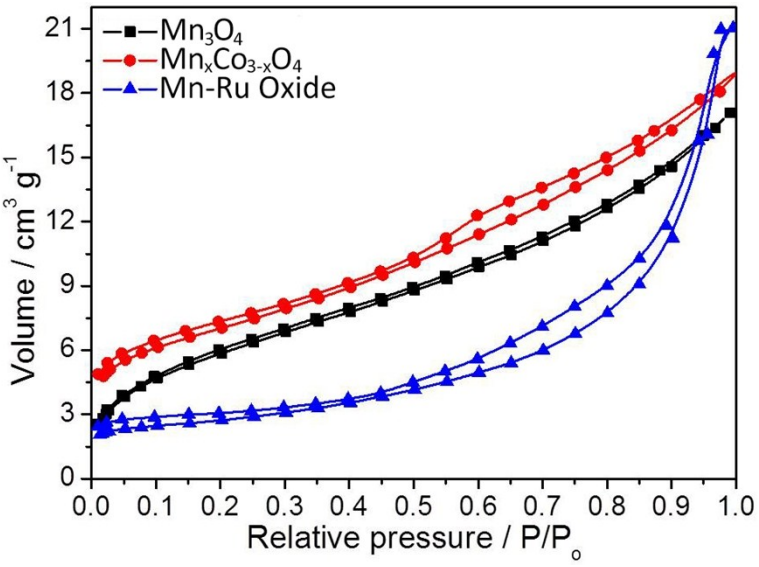

Figure S6 N_2 gas adsorption-desorption isotherms of Mn_3O_4, $Mn_xCo_{3-x}O_4$, and Mn-Ru oxide.

Figure S7

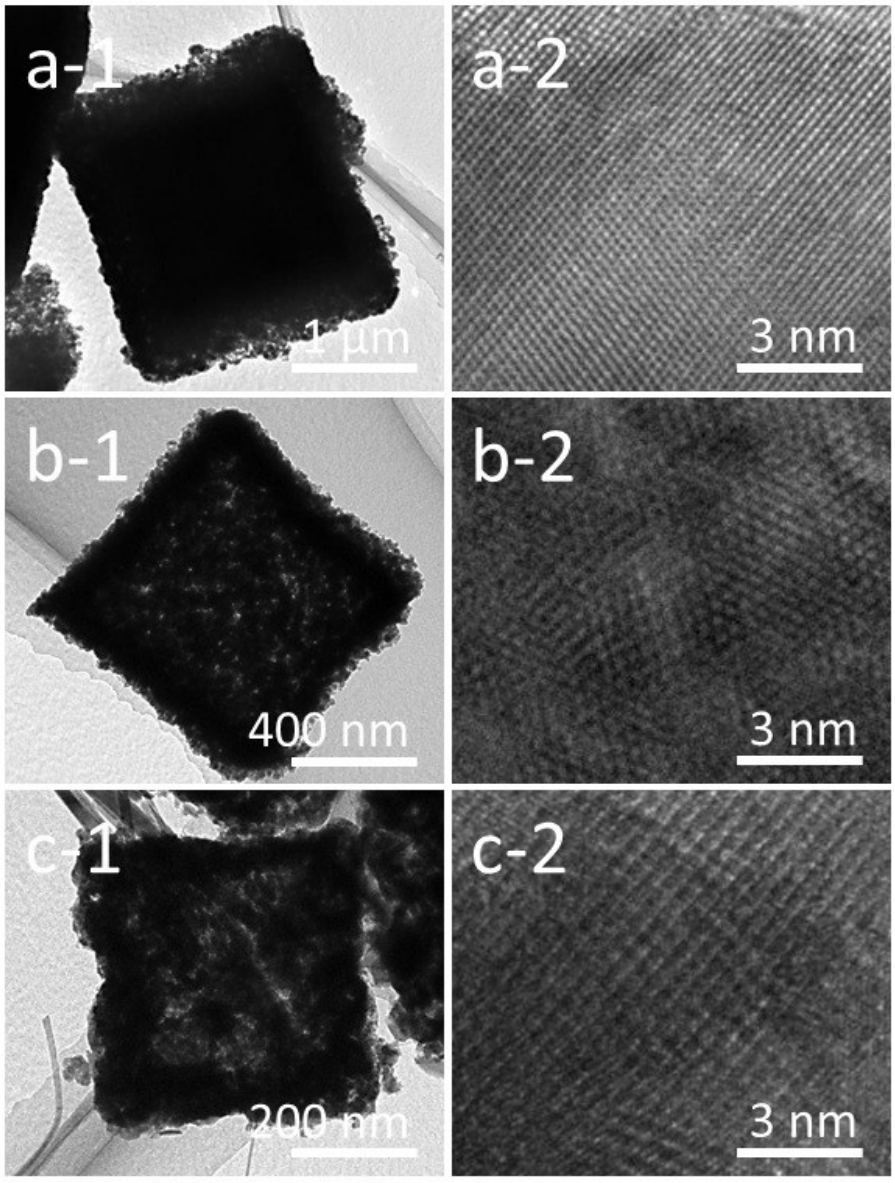

Figure S7 TEM and HRTEM images of the corresponding metal oxides prepared from (a) MnCNMn, (b) MnCNCo, and (c) MnCNRu PBAs.

Figure S8

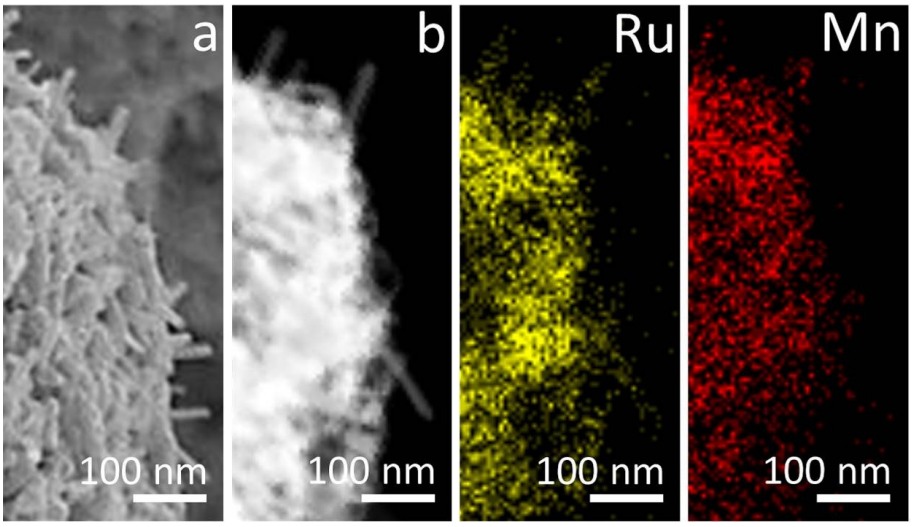

Figure S8 (a) SEM image and (b) HAADF-STEM images and the corresponding elemental mapping of the Mn-Ru oxides prepared from MnCNRu PBAs.

Figure S9

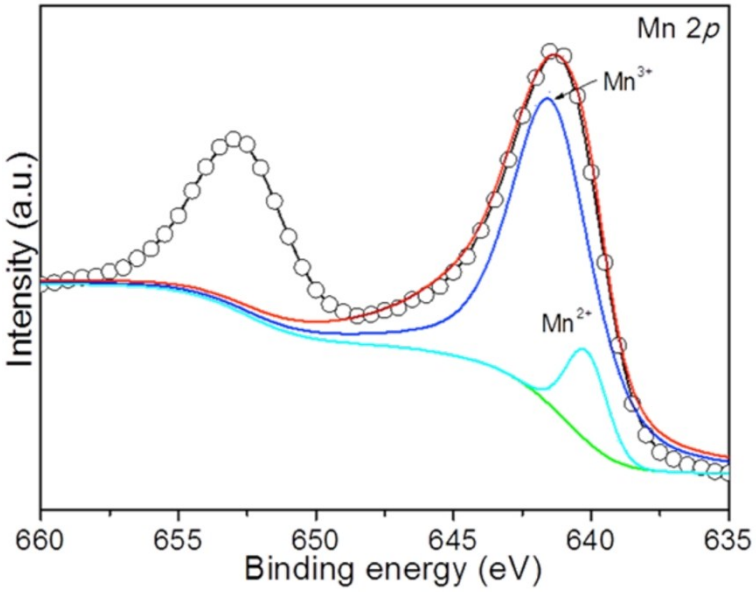

Figure S9 XPS spectra centered on Mn 2*p* in the Mn-Ru oxide.

Figure S10

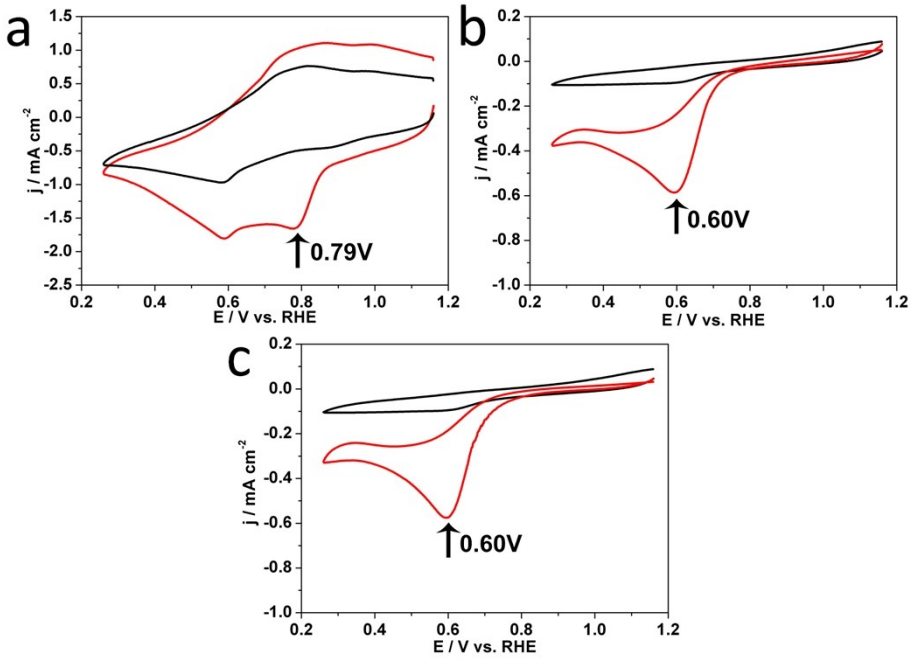

Figure S10 CV curves obtained under (black plot) N_2- and (red plot) O_2-saturated 0.1 M KOH catalyzed by (a) Mn oxide, (b) Mn-Co oxide, and (c) Mn-Ru oxide prepared from MnCNMn, MnCNCo, and MnCNRu PBAs, respectively.

Figure S11

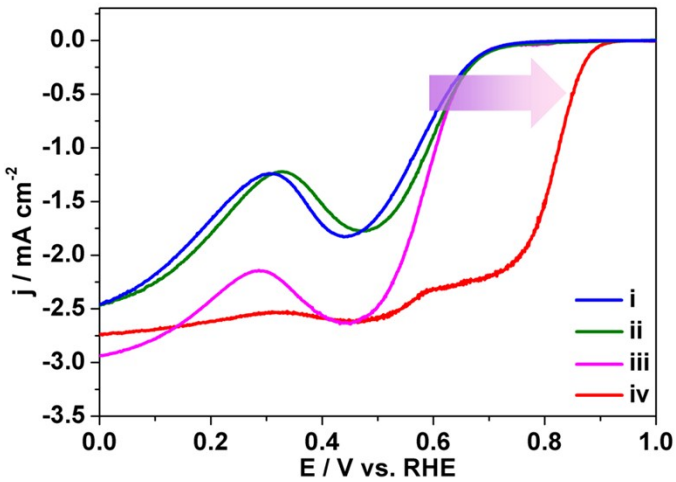

Figure S11 ORR polarization curves of (i) Mn oxide prepared from MnCNMn, (ii) Mn-Co oxide prepared from MnCNCo, (iii) commercially available RuO_2, and (iv) Mn-Ru oxide prepared from MnCNRu.

Figure S12

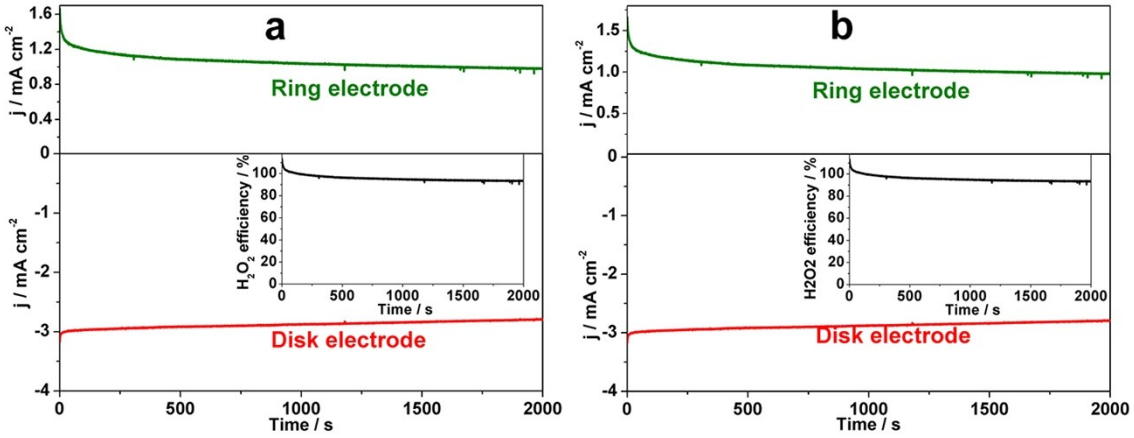

Figure S12 Chronoamperometric curves obtained at disk and ring electrodes at different constant potentials: (a) 0.65V and (b) 0.55V. The measurements were carried out in O_2-saturated 0.1M KOH at a rotation speed of 1600 rpm. The corresponding H_2O_2 production efficiencies were shown in the insets.

Figure S13

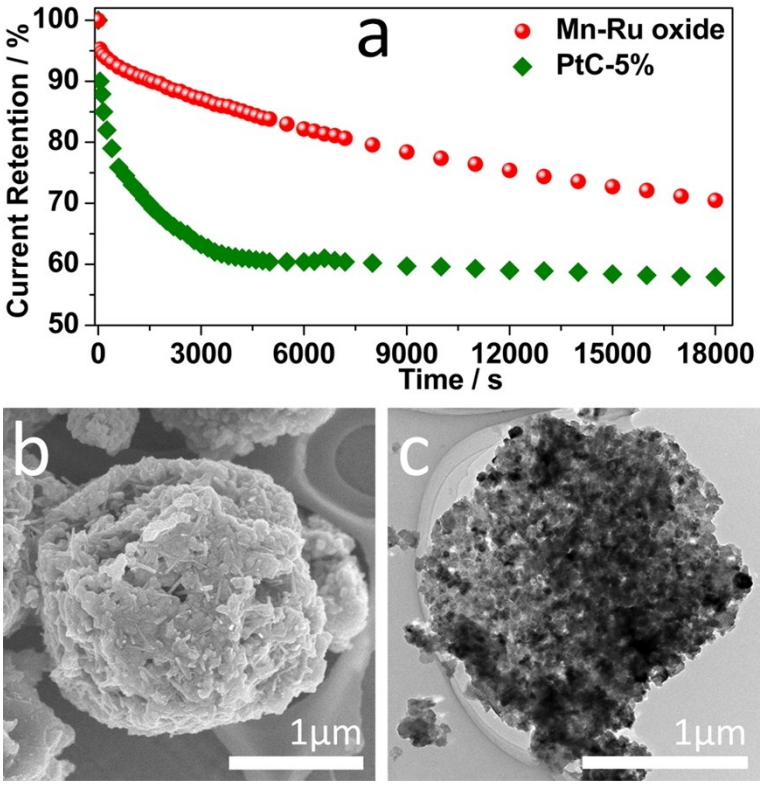

Figure S13 (a) Current retention plot during chronoamperometric measurements for the Mn-Ru oxide and commercially available PtC-5% catalysts. (b) SEM and (c) TEM images of the Mn-Ru oxide after long-term stability measurement.

Table S1 Comparison between the electrocatalytic activity toward ORR of our catalysts and other previously reported materials. *n* is the number of electron transferred during the ORR.

Sample information	Electrolyte	Onset potential* (mV *vs.* RHE)	*n*	References
Mn-Ru oxide	0.1M KOH	910	2.0	Present work
$Mn_xCo_{3-x}O_4$	0.1M KOH	762	2.0	Present work
Mn_3O_4	0.1M KOH	762	2.0	Present work
Mesoporous N-doped carbon	0.1M KOH	730	2.6	Adv. Funct. Mater. 2012, 22, 4584
Reduced graphene oxide	0.1M KOH	810	2.7	Chem. Commun. 2013, 49, 6334
N-doped graphene	0.1M KOH	800	2.7	Nat. Mater. 2011, 10, 780
$CoMn_2O_4$	0.1M KOH or KCl	780	2.9	Nat. Chem. 2011, 3, 79
Co_2MnO_4	0.1M KOH or KCl	850	3.3	Nat. Chem. 2011, 3, 79
$Co_xMn_{3-x}O_4$	0.1M KOH or KCl	860	3.4	Nat. Chem. 2011, 3, 79
Porous calcium-manganese oxide ($Ca_2Mn_3O_8$) microspheres	0.1M KOH	850	3.5	Chem. Sci. 2013, 4, 368
$Co_xMn_{3-x}O_4$	0.1 M KOH or KCl	880	3.7	Nat. Chem. 2011, 3, 79
Co_3O_4/graphene composite	1.0M KOH	864	3.7	J. Am. Chem. Soc. 2012, 134, 3517
Manganese oxide containing mesoporous N-doped carbon	0.1M KOH	810	3.8	Adv. Funct. Mater. 2012, 22, 4584
Flower-like manganese oxide on reduced graphene oxide	0.1M KOH	840	3.8	Chem. Commun. 2013, 49, 6334
Spinel $MnCo_2O_4$/ graphene composite	1.0M KOH	885	3.9	J. Am. Chem. Soc. 2012, 134, 3517
Co_3O_4 nanocrystals on graphene	0.1M KOH	880	3.9	Nat. Mater. 2011, 10, 780
Iron-based catalyst (Fe-N/C)	0.1M KOH	700	3.9	Nat. Mater. 2011, 10, 780
Platinum/carbon	0.1M KOH or KCl	50	3.9	Nat. Chem. 2011, 3, 79
Spinel $MnCo_2O_4$ nanoparticles + graphene sheet mixture	1.0M KOH	845	4.0	J. Am. Chem. Soc. 2012, 134, 3517
N-doped graphene sheets	1.0M KOH	830	4.0	J. Am. Chem. Soc. 2012, 134, 3517
Manganese oxide (β-MnO_2)	0.1M KOH	800	4.0	Angew. Chem. Int. Ed. 2013, 52, 2474
Layer-by-layer structured NiO-GO nanocomposite	0.1M KOH	860	---	Chem. Commun. 2015, 51, 16409
Cobalt and nitrogen-functionalized graphene	0.1M KOH	862	---	J. Mater. Chem. A 2013, 1, 3593

*: The potential in the present study was firstly recorded by using Ag/AgCl electrode. After the calibration of the reference electrode with respect to the reversible hydrogen electrode (RHE), the obtained potentials were converted to the scale against RHE.